

The Optimization of Rotary Bending Die Process: Criteria for the Metal Sheet Angles and Springback Effects

Vu Duc Quang

Faculty of Mechanical Engineering, University of Economics-Technology for Industries, Hanoi City, Vietnam

vuquang@uneti.edu.vn (corresponding author)

Received: 23 November 2024 | Revised: 24 December 2024 and 2 January 2025 | Accepted: 4 January 2025

Licensed under a CC-BY 4.0 license | Copyright (c) by the authors | DOI: <https://doi.org/10.48084/etasr.9706>

ABSTRACT

Rotary die bending enables the precise fabrication of sheet metal components across various bending angles, offering high dimensional accuracy, structural stability, and reduced springback. This study employs explicit and implicit numerical simulations using the Abaqus software to analyze the rotary die bending process and springback behavior of SUS304 stainless steel sheets. Five key criteria are investigated: desired angle post-springback (α_2), springback factor (k_s), forming stress (Von Mises) at the required bending angle (S_r), residual stress (Von Mises) after springback (S_b), and equivalent plastic strain (PEEQ). These criteria enable accurate predictions of material behavior during rotary die bending, including elastic-plastic deformation and stress distribution. The insights gained support a more flexible design process, enhance the precision of sheet metal bending, and ensure that the final product meets the specified requirements. This research serves as a valuable reference for professionals working with sheet metal components made from various metals and bimetal sheets. Additionally, it informs strategies to mitigate or eliminate residual stress in bent parts, improving reliability and manufacturability.

Keywords-rotary die bending; bending angle; SUS304 stainless steel sheet; springback; 3D numerical simulation

I. INTRODUCTION

Sheet metal bending is a widely utilized manufacturing process in which force is applied to a workpiece, causing the material within the bend allowance zone to undergo elastic-plastic deformation. This results in a specific bend radius or angle [1-2]. The versatility of this process allows for the production of a wide range of products, from simple to complex shapes, including vehicle body panels, electronic enclosures, and brackets [1-3]. Presses are commonly used to apply the necessary bending force, which can exceed 100 tons, enabling the bending of metal sheets of various thicknesses [3-4]. Among the different sheet metal bending techniques, rotational die bending stands out for its effectiveness in achieving precise bend angles while maintaining the desired bend radius [2, 4]. This method is extensively employed in the sheet metal industry to produce high-quality final products. A common challenge in sheet metal bending is springback, a phenomenon where the material partially reverts to its original shape after the bending force is removed, as illustrated in Figure 1. This elastic recovery causes deviations from the intended bend angle and radius, primarily due to the release of residual stresses within the material [1]. The springback factor, denoted as k_s , plays a critical role in predicting the extent of springback and calculating the final bend radius accurately [1-2, 5-8]. Equation (1) determines this factor accounting for the

material properties and bending parameters. Recent studies have focused on refining k_s to enhance the precision of the springback predictions and bend radius calculations [4, 5, 7, 8].

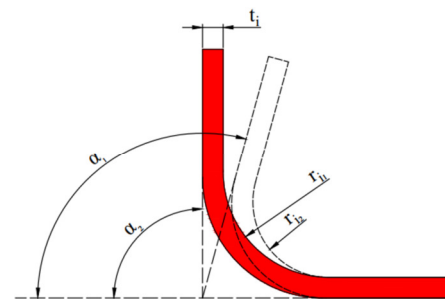


Fig. 1. Elastic recovery after bending.

$$k_s = \frac{\alpha_2}{\alpha_1} = \frac{r_{i1} + 0.5 \times t_i}{r_{i2} + 0.5 \times t_i} \quad (1)$$

where α_1 is the angle at the die (required bending angle, °), α_2 is the angle at the workpiece (desired angle after springback, °), t_i is the sheet metal thickness (mm), r_{i1} is the inside radius at the die (mm), and r_{i2} is the inside radius at the workpiece (mm).

Scientific research has advanced various methods to predict and compensate for the springback phenomena in the sheet

metal forming processes. One notable approach involves the use of a multilayer perceptron-based artificial neural network combined with a genetic algorithm to predict springback in cold-rolled anisotropic steel sheets [9]. This technique has demonstrated enhanced accuracy in forecasting the springback behavior, facilitating an improved control in manufacturing settings. Another study introduced a springback prediction model for AZM120 metal sheets, validated through both experimental procedures and numerical simulations [10]. By applying the elastic-plastic bending theory alongside numerical simulation, the study assessed the forming performance of the sheet metal, leading to more precise springback predictions. Recent comparative research evaluated the straight flanging and rotary die bending concerning springback. The findings revealed that the rotary die bending produced smaller springback values with significantly less variability compared to the straight flanging, making it a promising choice for applications requiring high precision [11]. Additionally, the combination of Finite Element Method (FEM) simulations with experimental V-bending processes has been utilized to investigate the normal and adjusted springback parameters [12]. This integrated approach enables an accurate parameter evaluation, improving both the predictability and control of springback in sheet metal forming. Furthermore, advancements in the Finite Element Analysis (FEA) have enhanced the accuracy of simulations for the V-bending process, providing valuable insights into the prediction and mitigation of springback effects.

Bending force is a crucial parameter in the bending process and in selecting the appropriate press capacity. Authors in [8] combined numerical simulations and experiments on aluminum AA1100-O and medium carbon steel sheet-grade SPCC, and introduced a V-die bending force formula that offers improved accuracy over earlier models [8]. The study utilized FEM to analyze the V-die bending mechanism, leading to the development of a new formula. The laboratory experiments validated the FEM results, confirming the formula's precision with an error margin of approximately 5% compared to the experimental data. The forming stress at the end of the upper die stroke and the residual stress after the upper die withdrawal were examined. Residual stress, which persists in a material after the external force is removed, has a significant impact on the performance and durability of the formed parts [2, 4-5]. It influences the structural integrity, fatigue life, and susceptibility to stress corrosion cracking. Using the LS-DYNA software, the residual stresses in monolithic aluminum sheets and aluminum/polypropylene/aluminum sandwich laminates were analyzed following the springback of a U-channel formed by draw bending. The results revealed that both forming stresses and residual stresses in the sandwich laminates were lower than those in the monolithic aluminum, which was of equivalent thickness [13]. Numerous commercial software packages are now available for the 3D numerical simulation of the sheet metal forming processes, including ABAQUS, LS-DYNA, ANSYS, COMSOL, DD3IMP, PAM-STAMP, and AUTOFORM. These tools are instrumental in predicting and addressing issues, such as springback, thinning/thickening, buckling risks, and internal stresses. By leveraging these technologies, manufacturers can enhance the

efficiency and quality of the sheet metal forming processes [14-19].

This article examines five output criteria in the rotary bending process for forming the elastic-plastic deformation of SUS304 sheet blanks. These criteria are the desired angle at the workpiece after springback (α_{si}), the springback factor (k_{si}), forming stress (Von Mises) at the required bending angle (S_r), residual stress (Von Mises) after springback (S_b), and the equivalent plastic strain at integration points ($PEEQ$). The study employs 3D numerical simulations using the Abaqus software, angle measurements via AutoCAD Mechanical, and mathematical analyses with Microsoft Office tools. The results are analyzed to predict the elastic-plastic deformation behavior of SUS304 sheet blanks. This analysis underscores several potential applications of the study, including the optimization of the tool and process parameters, cost savings and scrap reduction, improved part quality, and the identification of critical areas in the sheet metal forming process.

II. MATERIALS AND METHODS

A. Original Sheet Blank and Rotary Die Bending Model

The SUS304 stainless steel sheet blank with a length of $l_0 = 100$ mm, a width of $w_0 = 100$ mm, and a thickness of $t_0 = 2$ mm, is geometrically modeled for the numerical simulation, as can be seen in Figure 2. The rotary die bending model, depicted in Figure 3, consists of five key components: the upper die, lower die, rocker, rocker holder, and the sheet blank. This model was developed using the Abaqus software to analyze five output criteria during the formation of nine distinct bending angle samples. The mechanical properties of SUS304 stainless steel, used for the sheet blank in the FEM simulation, are detailed in Table I [20-21].

TABLE I. MATERIAL PROPERTIES OF SUS304 SHEET BLANK

Material properties	Value
Temperature (°C)	24
Density, ρ (kg/m ³)	7850
Young's modulus, E (GPa)	193
Hardening coefficient, K (MPa)	1275
Work hardening exponent, n	0.45
Poisson's ratio, ν	0.29
Yield strength (MPa)	226.3
Ultimate tensile strength (MPa)	560
Elongation (%)	45

B. Numerical Simulation

The explicit FEM was employed to simulate the 3D rotary die bending process in the Abaqus software, as portrayed in Figure 3. The upper die, lower die, and rocker holder were defined as rigid surfaces, while the rocker was modeled as an elastic body to replicate the actual boundary conditions and enhance the accuracy of the forming process. The sheet blank material was defined as elastic-plastic, assuming an isotropic hardening behavior for its plasticity. For the meshing settings, the sheet blank utilized hexagonal (hexa) mesh elements, structured deploying the default technique selection. Similarly, the rocker was meshed using hex elements, but with the sweep method as the meshing technique. The lower die was fixed in

position, while the upper die moved along the OY axis, corresponding to nine distinct tests ranging from $OY = -7.0$ mm (Test 1) to $OY = -37.5$ mm (Test 9), as detailed in Table II.

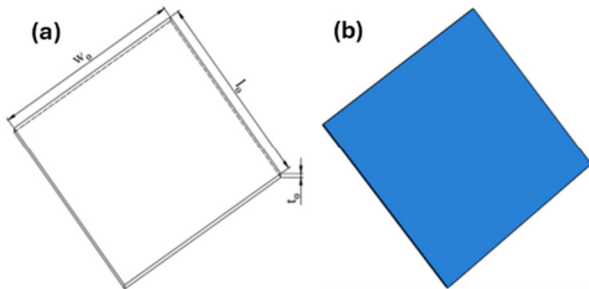


Fig. 2. (a) Shell blank, (b) its geometrical modeling.

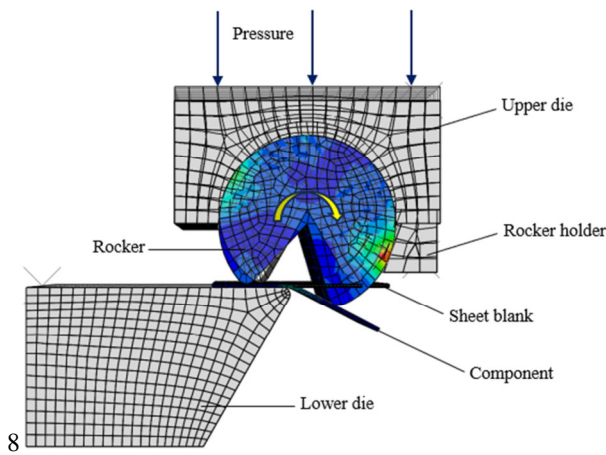


Fig. 3. Assembly and mesh modules in rotary bending dies process analysis.

TABLE II. BENDING ANGLE SAMPLES FOR ANALYZING FIVE OUTPUT CRITERIA

Test	OY [mm]	α_i [°]	Five output criteria
1	-7.0	23	(1) Desired angle at the workpiece after springback: α_{si}
2	-11.0	38	(2) Springback factor: k_{si}
3	-14.5	53	(3) Forming stress-Von Mises at required bending angle: S_r
4	-18.0	66	(4) Residual stress-Von Mises after springback: S_b
5	-22.0	80	(5) Equivalent plastic strain at integration points: $PEEQ$
6	-25.0	92	
7	-28.5	97	
8	-33.0	110	
9	-37.5	117	

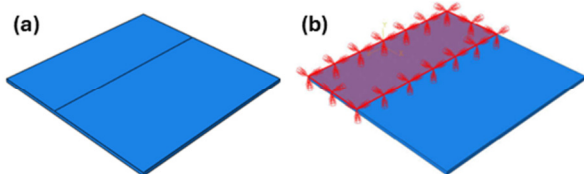


Fig. 4. Boundary condition settings in the load module for 3D simulation of springback behavior.

The rocker holder was tied to the upper die to maintain alignment during the simulation. The contact interactions were modeled using Coulomb's friction law, with friction coefficients (μ) having been applied to the relevant contact

pairs based on previous studies. The friction coefficient between the sheet blank and the rocker, as well as between the sheet blank and the lower die, was set to 0.3. For the interactions between the rocker and the upper die, and between the rocker and the rocker holder, the friction coefficient was set to 0.1 [1, 7]. During the springback behavior analysis, only the sheet blank is retained in the simulation, appearing as the blue material illustrated in Figure 4. The initial fixing area on the sheet blank is marked in pink, while the final fixing area is highlighted in red, as shown in Figure 4. The four tool components -the upper die, lower die, rocker holder, and rocker- are removed for clarity, allowing the focus to remain on the sheet blank and its deformation.

III. RESULTS AND DISCUSSION

A. Desired Angle at the Workpiece-After Springback, α_{si}

Springback refers to the geometric change that occurs in a component after the forming process, when the material is released from the forces applied by the forming tool. This phenomenon, known as reverse elasticity, takes place in the bending allowance zone. In this zone, the material above the neutral axis is compressed, while the material below the neutral axis is stretched. As a result, the desired bending angle (α_i) of the component becomes smaller than the required bending angle (α_i), as observed in Figure 5.

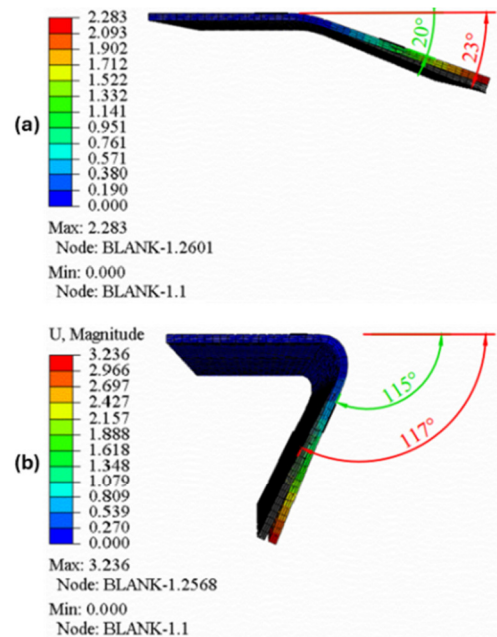


Fig. 5. Spatial displacement at nodes U (mm) on the part during the reverse elasticity process: (a) Test 1, (b) Test 9.

Figure 6 illustrates the required bending angles (α_i) and the corresponding desired angles (α_{si}) after each test. Specifically, the nine required angle samples (α_i , indicated in red in Figure 5) are arranged in an increasing order from α_1 to α_9 . Similarly, the bending angles after reverse elasticity (α_{si} , indicated in green in Figure 5) are also presented in an increasing order from α_{s1} to α_{s9} . These measurements were obtained using the

AutoCAD Mechanical software. The reverse elasticity angle ($\Delta\alpha = \alpha_i - \alpha_{si}$) for the nine angle samples is quite consistent, with an average value of $\Delta\alpha_a = 2.33^\circ$ for SUS304 stainless steel sheets with a thickness of $t_0 = 2$ mm. It is important to note that for SUS304 stainless steel sheets with thicknesses other than $t_0 = 2$ mm, the springback angle ($\Delta\alpha_a$) may vary.

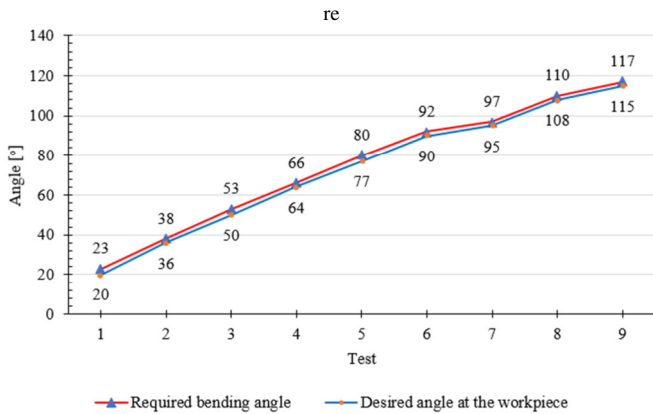


Fig. 6. Comparison chart of the desired angle α_{si} with the required bending angle α_i on the component.

B. Springback Factor: k_{si}

Figure 7 portrays the springback factor (k_{si}) for the nine investigated angle samples. The data are presented in an increasing order, showing a general upward trend in the springback factor as the bending angle increases, albeit with minor fluctuations. The springback factor can be predicted using the natural logarithm, derived from the data:

$$k_{si}(\alpha_{si}) = 0.0584 \ln(\alpha_{si}) + 0.714 \quad (2)$$

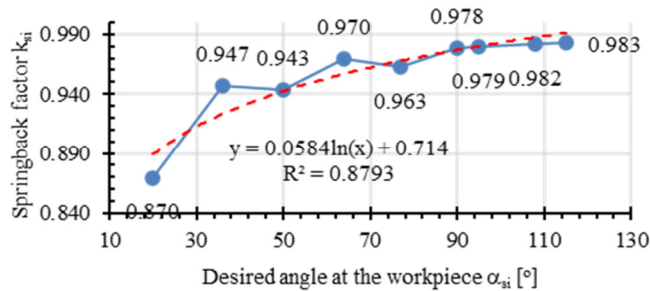


Fig. 7. The colleration of springback factor k_{si} with the desired bending angle at the workpiece α_{si} .

C. Forming Von Mises Stresses at the required bending Angle: S_r and Residual Von Mises Stresses after Springback: S_b

The forming stress at the end of the upper die and rocker stroke, as well as the residual stress at the end of the upper die and rocker withdrawal stroke, are numerically determined using the Abaqus software. The through-thickness stress distribution is established through an explicit forming simulation, followed by the determination of the through-thickness residual stress distribution via an implicit springback

simulation. During the rotary die bending process, pure bending characteristics are generated in the bending allowance zone, while reversed bending characteristics occur in the unclamped leg. This is clearly illustrated by the color distribution of the forming stress S_r and the residual stress S_b in Figure 8. The forming stress S_r exhibits a wide range of values, primarily concentrated in the bending allowance zone. Notably, the stretched grain side has a broader stress distribution compared to the compressed grain side, as can be seen in Figures 8(a) and 8(c). In contrast, the residual stress S_b also displays a broad distribution, mainly concentrated in the bending allowance zone. However, the values of the residual stress are significantly lower than those of the forming stress, with similar values obtained on both the stretched and compressed grain sides, as displayed in Figures 8(b) and 8(d). Based on the comparative data of the four parameters, the maximum forming stress S_{r-max} , the maximum residual stress S_{b-max} , yield strength, and ultimate tensile strength, presented in Figure 9, it can be observed that the maximum forming stress S_{r-max} increases significantly from 318 MPa for the angle sample 1 ($\alpha_1 = 23^\circ$) to 432 MPa for the angle sample 8 ($\alpha_8 = 110^\circ$), before sharply decreasing to 379 MPa for the angle sample 9 ($\alpha_9 = 117^\circ$). All these stress values are lower than the ultimate tensile strength, 560 MPa, and higher than the yield strength, 226.3 MPa. For the angle samples undergoing reverse elasticity, the maximum residual stress S_{b-max} tends to decrease sharply and fall below the yield strength. Specifically, for the angle sample 2 ($\alpha_{s2} = 36^\circ$), the minimum residual stress value is 157 MPa, while for the angle sample 9 ($\alpha_{s9} = 115^\circ$), the maximum residual stress value is 276 MPa, which exceeds the yield strength of 226.3 MPa. Notably, in the angle sample 9, this higher residual stress value can be explained by the phenomenon of deformation hardening during the forming process. The forming stress for sample 9 is 379 MPa, which is only slightly higher than the forming stress of 359 MPa for the angle sample 2. However, the residual stress in sample 9 is 276 MPa, significantly greater than the 157 MPa observed for sample 2.

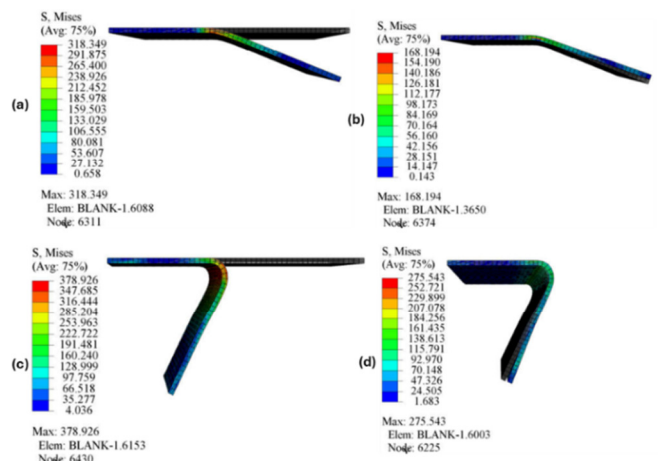


Fig. 8. Distribution of forming stress S_r and residual stress S_b on the bending component: (a) required bending angle sample $\alpha_1 = 23^\circ$, (b) desired bending angle sample $\alpha_{s1} = 20^\circ$, (c) required bending angle sample $\alpha_9 = 117^\circ$, (d) desired bending angle sample $\alpha_{s9} = 115^\circ$.

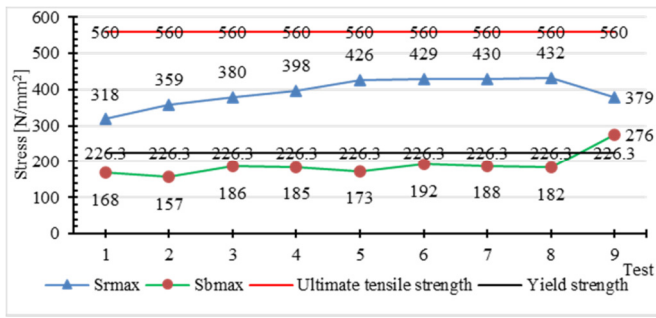


Fig. 9. Maximum forming stress and maximum residual stress in the bending component at the required bending angles and desired bending angles compared with the yield stress and ultimate tensile stress of the material.

Eliminating or minimizing the residual stress distribution throughout the thickness of the SUS304 sheet material after bending is crucial to ensure the dimensional stability and mechanical performance of the final product. This can be achieved through several techniques, such as heat treatment, vibration stress relief, and natural aging [22-23].

D. Equivalent Plastic Strain at Integration Points: PEEQ

The equivalent plastic strain at the integration points (PEEQ) distributed along the bending part, corresponds to the required bending angle α_i and the desired bending angle α_{si} . This strain is concentrated exclusively in the bend allowance zone, as detailed in Figure 10.

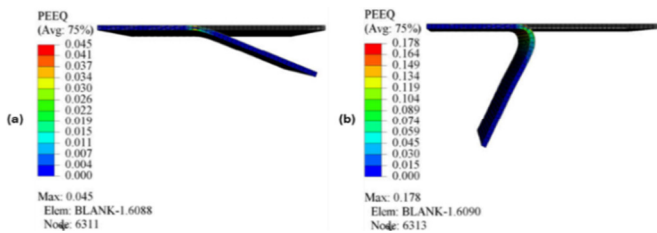


Fig. 10. PEEQ distribution on the bending component for the required bending angles: (a) $\alpha_1 = 23^\circ$, (b) $\alpha_9 = 117^\circ$.

The maximum PEEQ value ($PEEQ_{max}$, shown in red in Figure 10, increases with the required bending angle α_i ; for the bending angle sample 1 ($\alpha_1 = 23^\circ$), $PEEQ_{max-\alpha_1} = 0.045$, and for the bending angle sample 9 ($\alpha_9 = 117^\circ$), $PEEQ_{max-\alpha_9} = 0.178$. All $PEEQ_{max}$ values are significantly smaller than 1, indicating that the material in the bending allowance zone undergoes elastic-plastic deformation within a safe range, with a uniform thickness of the component at $t_i = 2$ mm. Through the numerical simulation, the potential for sheet failure can be predicted when $PEEQ_{max} \geq 1.0$.

Based on the $PEEQ_{max}$ coefficient data, presented in Figure 11, for the required bending angle samples α_i , the relationship between $PEEQ_{max}$ and α_i can be predicted using the quadratic equation with a variance of $R^2 = 0.9786$:

$$PEEQ_{max(\alpha_i)} = -3E - 6 \times \alpha_i + 0.0017 \times \alpha_i^2 + 0.0099 \quad (3)$$

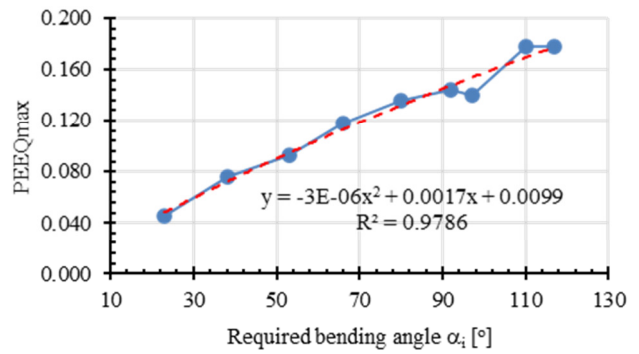


Fig. 11. Colleration of $PEEQ_{max}$ coefficient with the required bending angle α_i .

IV. CONCLUSIONS

This study successfully utilized the Finite Element Method (FEM) to simulate the 3D rotary die bending process, enabling the prediction of the elastic-plastic deformation and the associated springback behavior of SUS304 sheet blanks using the Abaqus software. The analysis of nine bending angle samples yielded the following significant findings across five key output criteria:

- **Desired bending angle (α_{si}):** The desired bending angle (α_{si}), was consistently smaller than the required bending angle α_i , with an average angular difference of approximately $\Delta\alpha_i = 2.33^\circ$.
- **Springback factor (k_{si}):** The springback exhibited a gradual convergence towards 1.0.
- **Maximum forming stress (S_{r-max}):** The maximum forming stress increased with the required bending angle up to $\alpha_8 = 110^\circ$. For $\alpha_i > \alpha_8$, it decreased due to intensified material deformation hardening.
- **Maximum residual stress (S_{b-max}):** The maximum residual stress remained relatively stable and below the yield stress (226.3 MPa) for bending angles up to $\alpha_8 = 110^\circ$. However, for $\alpha_i > \alpha_8$, it exceeded the yield stress due to enhanced material deformation hardening.
- **Equivalent Plastic Strain ($PEEQ_{max}$):** The coefficient $PEEQ_{max}(\alpha_i)$ gradually increased to 0.2, well below the critical value of 1.0, and was determined as the required bending angle.

These findings offer engineers critical insights into the behavior of sheet metal materials during rotary die bending across varying angles. By improving the ability to predict and compensate for phenomena, such as springback, this research facilitates an enhanced geometrical shape accuracy, improved workability, and increased manufacturing efficiency. The methodologies and results presented in the current paper provide a robust foundation for optimizing the rotary die bending process, supporting more effective and reliable manufacturing practices.

REFERENCES

- [1] C. V. Nielsen and P. A. F. Martins, *Metal Forming: Formability, Simulation, and Tool Design*, London, England: Academic Press, 2021.
- [2] Schuler, *Metal Forming Handbook*, Berlin, Germany: Springer, 1998.
- [3] J. Hu, Z. Marciniak, and J. Duncan, *Mechanics of Sheet Metal Forming*, 2nd ed. Oxford, United Kingdom: Butterworth-Heinemann, 2002.
- [4] N. M. Dang, N. N. Huynh, and P. H. Duong, *Sheet metal forming technology*, 1st ed. Hanoi, Vietnam: Science and Technology Publishing House, 2006.
- [5] K. Lange, *Handbook of metal forming*, 1st ed. New York, USA: McGraw-Hill Inc, 1985.
- [6] Y. E. Ling, H. P. Lee, and B. T. Cheok, "Finite element analysis of springback in L-bending of sheet metal," *Journal of Materials Processing Technology*, vol. 168, no. 2, pp. 296–302, Sep. 2005, <https://doi.org/10.1016/j.jmatprotec.2005.02.236>.
- [7] W. Phanitwong and S. Thipprakmas, "Development of anew spring-back factor for a wiping die bending process," *Materials & Design*, vol. 89, pp. 749–758, Jan. 2016, <https://doi.org/10.1016/j.matdes.2015.10.031>.
- [8] K. Doungmarda and S. Thipprakmas, "A New Bending Force Formula for the V-Die Bending Process," *Metals*, vol. 13, no. 3, Mar. 2023, Art. no. 587, <https://doi.org/10.3390/met13030587>.
- [9] T. Trzepieciński and H. G. Lemu, "Improving Prediction of Springback in Sheet Metal Forming Using Multilayer Perceptron-Based Genetic Algorithm," *Materials*, vol. 13, no. 14, Jan. 2020, Art. no. 3129, <https://doi.org/10.3390/ma13143129>.
- [10] C. Chen, J. Gong, Y. Chen, and J. Wang, "A prediction model for bending springback of AZM120 sheet metal and mechanical compensation of CNC automatic panel bender," *The International Journal of Advanced Manufacturing Technology*, vol. 116, no. 9, pp. 3325–3337, Oct. 2021, <https://doi.org/10.1007/s00170-021-07606-1>.
- [11] H. Livatyali, S. E. Turan, F. Birol, and M. Türköz, "Experimental comparison of straight flanging and rotary die bending based on springback," *The International Journal of Advanced Manufacturing Technology*, vol. 120, no. 7, pp. 4373–4386, Jun. 2022, <https://doi.org/10.1007/s00170-022-09020-7>.
- [12] S. Thipprakmas, "Spring-back factor applied for V-bending die design," *Journal of Advanced Mechanical Design, Systems, and Manufacturing*, vol. 14, no. 3, 2020, Art. no. JAMDSM0037, <https://doi.org/10.1299/jamdsm.2020jamdsm0037>.
- [13] C. Kella and P. K. Mallick, "Residual Stress Distribution in Aluminum/Polypropylene/Aluminum Sandwich Laminates in U-Channel Draw Bending," *Journal of Materials Engineering and Performance*, vol. 33, no. 15, pp. 7616–7625, Aug. 2024, <https://doi.org/10.1007/s11665-024-09421-7>.
- [14] T. Trzepieciński, F. dell'Isola, and H. G. Lemu, "Multiphysics Modeling and Numerical Simulation in Computer-Aided Manufacturing Processes," *Metals*, vol. 11, no. 1, Jan. 2021, Art. no. 175, <https://doi.org/10.3390/met11010175>.
- [15] D. Banabic, *Sheet Metal Forming Processes: Constitutive Modelling and Numerical Simulation*, New York, United States: Springer Science & Business Media, 2010.
- [16] H. G. Lemu and T. Trzepieciński, "Numerical and Experimental Study of Frictional Behavior in Bending Under Tension Test," *Journal of Mechanical Engineering*, vol. 59, no. 1, pp. 41–49, Jan. 2013, <https://doi.org/10.5545/sv-jme.2012.383>.
- [17] A. M. F. Pimentel, J. L. de Carvalho Martins Alves, N. M. de Seabra Merendeiro, and D. M. F. Vieira, "Comprehensive benchmark study of commercial sheet metal forming simulation softwares used in the automotive industry," *International Journal of Material Forming*, vol. 11, no. 6, pp. 879–899, Nov. 2018, <https://doi.org/10.1007/s12289-018-1397-4>.
- [18] W. Liu, X. Zhang, and P. Hu, "Developments of multi-step simulations in sheet metal forming processes," *The International Journal of Advanced Manufacturing Technology*, vol. 93, no. 1, pp. 1379–1397, Oct. 2017, <https://doi.org/10.1007/s00170-017-0627-0>.
- [19] M. A. Ablat and A. Qattawi, "Numerical simulation of sheet metal forming: a review," *The International Journal of Advanced Manufacturing Technology*, vol. 89, no. 1, pp. 1235–1250, Mar. 2017, <https://doi.org/10.1007/s00170-016-9103-5>.
- [20] Q. V. Duc, D. D. Van, T. N. Dac, and Q. N. Huu, "Quality comparison of Y-shape joints by tube hydroforming with and without counterforce," *EUREKA: Physics and Engineering*, no. 4, pp. 46–56, Jul. 2022, <https://doi.org/10.21303/2461-4262.2022.002256>.
- [21] Q. D. Vu, T. D. Nguyen, H. V. Dang, and D. T. Phan, "Effect of loading paths on hydroforming ability of stepped hollow shaft components from double layer pipes," *EUREKA: Physics and Engineering*, no. 4, pp. 143–154, Jul. 2023, <https://doi.org/10.21303/2461-4262.2023.002797>.
- [22] X. Zhu, X. Wang, and H. Wu, "Calculation method and analysis of residual stress in the strip bending roller straightening process," *Scientific Reports*, vol. 14, no. 1, Apr. 2024, Art. no. 9149, <https://doi.org/10.1038/s41598-024-59305-y>.
- [23] T.-D. Tran and P.-H. V. Nguyen, "Computation of Limit Loads for Bending Plates," *Engineering, Technology & Applied Science Research*, vol. 13, no. 2, pp. 10466–10470, Apr. 2023, <https://doi.org/10.48084/etasr.5671>.